analytical chemistry

Article

pubs.acs.org/ac

ESI-IM-MS and Collision-Induced Unfolding That Provide Insight into the Linkage-Dependent Interfacial Interactions of Covalently Linked Diubiquitin

Nicole D. Wagner,[†] David E. Clemmer,[‡] and David H. Russell*[,†]

[†]Department of Chemistry, Texas A&M University, College Station, Texas 77843, United States

[‡]Department of Chemistry, Indiana University, Bloomington, Indiana 47405, United States

Supporting Information

ABSTRACT: Understanding protein higher order structure and interfacial interactions is crucial to understanding protein binding motifs and cellular function, that is, an interactome. Polyubiquitylation is a post-translational modification that functions as a tag for a diverse array of cellular processes, wherein differences in chain length, branching, and linkage site encode different cellular functions. Investigation of covalently linked diubiquitin (diUbq) molecules specifically selects for the effect of covalent linkage site on the conformational preference of the molecule and the interfacial interactions between the subunits. Here, we report results for electrospray ionization ion mobility-mass spectrometry (ESI-IM-MS) and collision-induced unfolding (CIU) analysis of four diUbq ions to provide new understanding of the differences in subunit interfacial interactions and conformational preferences induced by the four most common covalent linkage sites. The specific hydrophobic patch interface adopted by K48-linked diUbq results in unique CIU fingerprints dominated by conformational broadening and primarily gradual unfolding, as opposed to the distinct transitions through gas-phase unfolding intermediates observed of K6-, K11-, and K63-linked diUbq. Comparison of the intermediate conformational families of K6-, K11-, and K63-linked diUbq suggests that K6- and K11-linked diUbq adopt a mixture of conformers stabilized by either electrostatic interactions or hydrophobic interactions involving the I36 hydrophobic patch. Furthermore, conditions favoring the partially folded A-state of monoubiquitin, that is, methanolic solution, induce conformational collapse and distinct unfolding intermediates for all four linkage types, providing an end-point at which all solution-phase conformational "memory" has been lost.

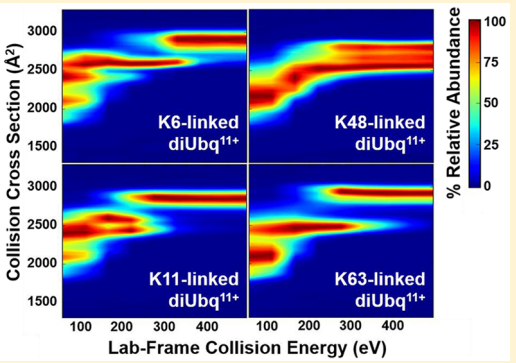

Many biological processes are attributable to specific protein−protein interactions. The majority of proteins function primarily as a subunit in a larger protein complex rather than as a single entity. In yeast cells, rough estimates suggest that the average protein may participate in 3−10 interactions with other binding partners.[1] Characterizing an interactome is challenging, particularly due to the dynamic and often transient nature of higher order structures. Electrospray ionization ion mobility-mass spectrometry (ESI-IM-MS) has established widespread applicability for evaluating the conformational preference of biological molecules.[2−5] IM-MS is capable of rapid characterization of heterogeneous conformational mixtures via separation of ions on the basis of their three-dimensional shape and charge, that is, their ion-neutral collision cross section (CCS). MS, tandem MS, and IM-MS have been used with moderate success for the characterization of protein complex identities and quaternary structure.[6−11] More recently, new applications of gas-phase activation methods have been applied to the characterization of complex quaternary structure, such as surface-induced dissociation and collision-induced unfolding (CIU).[9,12−14] CIU is the stepwise increase in the internal energy of the ion through collisional activation with a buffer gas and subsequent structural analysis using IM-MS. As such, CIU results in a gas-phase unfolding fingerprint that is often unique and representative of the ion's noncovalent interactions. CIU has been applied to examine differences in protein complex interfaces, intramolecular interactions, and lipid and anion binding-induced stabilization.[14−21]

Ubiquitin (Ubq) is a 76 amino acid protein with a highly conserved primary structure that has been studied extensively both in solution and as a solvent-free, gas-phase ion.[22−26] Despite transfer into the gas phase, low charge states of Ubq ions are known to exhibit CCS values similar to that reported for the native-fold in solution.[26−30] Ubq displays diverse biological functionality as a tag, that is, ubiquitylation, for cellular processes as defined by its oligomeric state; polyubiquitylation is a post-translational modification wherein a chain of Ubq subunits is covalently linked to a target molecule. Each Ubq subunit of a polyubiquitin (polyUbq) tag is linked through a specific

Received: July 25, 2017
Accepted: August 25, 2017
Published: August 25, 2017

ACS Publications © XXXX American Chemical Society

DOI: 10.1021/acs.analchem.7b02932
Anal. Chem. XXXX, XXX, XXX−XXX

isopeptide bond between the C-terminus of one subunit and an amino group of another subunit. The functionality of a specific polyUbq tag is encoded by its distinct quaternary structure and the resulting binding motif induced by differences in linkage site, chain length, and branching.[31−36] Ubq contains eight amino groups (seven lysine side chains and the N-terminus) that may form the covalent linkage, each encoding unique cellular functions. For example, K48-linked tetraUbq functions primarily as a tag for the proteosomal degradation of the target protein within the 26S proteasome complex.[31,37] The ubiquitin-proteasome pathway is used to degrade misfolded proteins and antigens;[38] furthermore, the dysfunction of this pathway is implicated in the pathogenesis of several neurodegenerative diseases.[39,40] K11-linked polyUbq is linked to regulation of cell division and mitosis,[41] whereas K63-linked tetraUbq is implicated in DNA repair,[42,43] inflammation,[44] immune response,[38] trafficking,[42] and antiviral response.[45] Both K48- and K63-linked polyUbq types have been implicated in the oncogenesis of several cancers and as such are a target for cancer therapy.[46]

Ubiquitin monomers (monoUbq) adopt highly stable, compact β-grasp fold structures, as characterized by NMR and X-ray crystallography,[22,47] and a high degree of this tertiary structure is maintained for each subunit of polyUbq, including the I44 (L8, I44, V70) and I36 (I36, L71, L73) hydrophobic patches.[35] Here, we examine four diUbq molecules linked through K6, K11, K48, and K63 to better understand the interfacial interactions induced by the different covalent linkage types; the most common linkage types in yeast cells are observed linked through the residues K48 (29.1%), K11 (28%), K63 (16.3%), and K6 (10.9%).[48] Under physiological conditions, K48-linked diUbq exists in equilibrium wherein conformers are stabilized by interactions of the I44/I44 hydrophobic patches or purely electrostatic interactions that expose the I44 patches for binding.[32,49,50] In more acidic environments, the electrostatic interface is reportedly preferred due to protonation of basic residues (K6, K11, R42, R72, and H68) in close proximity to the I44 patches and the resulting Coulombic repulsion.[50,51] Because of steric hindrance, K63-linked diUbq molecules cannot form interfacial interactions between the hydrophobic patches and instead occupy an ensemble of conformations including closed conformations stabilized by electrostatic interactions.[36,52] The conformational preferences of K6- and K11-linked diUbq are less well-defined. Two solution-phase conformers of K11-linked diUbq have been reported: one stabilized through I36/I36 interfacial interactions and the other through electrostatic interactions.[41,53−55] A single-crystal structure for K6-linked diUbq exhibiting I36/I44 interfacial interactions has been reported.[56] More recent NMR spectroscopy and small-angle neutron scattering (SANS) results have reported that a single structure is a woefully incomplete representation of the conformational space occupied by the different diUbq molecules.[57] Recent reports suggest that because the C-terminus of Ubq is inherently flexible, diubiquitin (diUbq) molecules adopt a dynamic ensemble of solution-phase conformations, and thus these single structures are likely an oversimplification of diUbq conformational preference and interfacial binding, further complicating potential analyses.[57,58]

Fenselau noted that characterizing the role of each linkage type is difficult: "The ubiquitin code is expected to correlate patterns of ubiquitination with the functional fates conveyed to protein substrates by conjugation. The code has been only partly deciphered because no suitable analytical method is available."[59]

Despite decades of research, few analytical methods are available for characterization of polyUbq covalent linkage types, most notably immunoprecipitation[60] and the use of linkage specific deubiquitinating enzymes (DUB);[61] however, both immunoprecipitation and the use of DUB enzymes suffer from a limited understanding in terms of linkage specificity, the lack of binding partners for all linkage types, and the ability to characterize homogeneous or branched polyUbq structures. Mass spectrometry fragmentation techniques have more recently been introduced for the characterization of polyUbq isomers.[62,63] We have recently reported the use of ESI-IM-MS and collision-induced unfolding (CIU) for the evaluation of the conformational preference and interfacial interactions observed for the noncovalent homodimer of Ubq through comparisons with K48- and K63-linked diUbq.[64] With current resolution limits, IMS alone was insufficient to differentiate the conformational preferences of K48- and K63-linked diUbq ions and the noncovalent dimer of Ubq; however, collision-induced unfolding (CIU) supplies an added dimension capable of differentiating dissimilar noncovalent interactions. The results suggest that the conformational preferences of K48- and K63-linked diUbq are differentiable using CIU; furthermore, noncovalent Ubq dimer ions exhibit noncovalent interfacial interactions and likely conformational preferences similar to those of K48-linked diUbq ions. Here, we report a more in-depth discussion of the conformational preferences observed for the four most common linkage types reported for polyUbq (K6-, K11-, K48-, and K63-linkages)[48] utilizing more intensive interpretation of diUbq ESI-IM-MS results and CIU fingerprints with the aid of solvent-induced denaturation.

EXPERIMENTAL SECTION

Sample Preparation. K6-, K11-, K48-, and K63-linked diubiquitin were purchased from R&D Systems Inc. (Minneapolis, MN). All were used without further purification. Each was dissolved in 18 MΩ water (Barnstead Easy Pure II, Thermo Scientific) and stored at −20 °C for later use. All solutions were prepared with a final concentration of 10 μM in either 99.9/0.1% (v/v %) water/formic acid or 49.9/50/0.1% (v/v %) water/methanol/formic acid.

ESI-IM-MS and CIU Analysis. ESI-IM-MS spectra were acquired using a Waters Synapt G2 HDMS mass spectrometer (Manchester, UK). Instrument conditions were chosen to minimize instrumental heating: sample cone, 10 V; extraction cone, 1 V; trap bias, 25 V; API gas flows, off; helium cell flow rate, 200 mL/min; IMS nitrogen flow rate, 60 mL/min; TWIMS wave height, 20 V; TWIMS wave velocity, 300 m/s.[30] CCS values were calibrated as previously described using reported values for acid and acetonitrile denatured ubiquitin, cytochrome c, and myoglobin.[65] All CCS profiles were normalized to the most abundant feature.

Different collision energies for CIU were imparted by changing the voltage drop between the exit of the quadrupole and the entrance to the TWIG-trap region filled with the collision gas argon. Note that a 5 V drop was necessary to maintain transmission through the trap and transfer regions and will be referred to as low collision energy. Reported lab-frame collision energies were calculated as the product of ion charge and acceleration voltage. CIUSuite was used to assemble all CIU heat maps from IM-MS spectra; the "compare" function of CIUSuite was used to produce difference plots, used to draw attention to differences in CIU heat maps, and to produce RMSD values, used to summarize those differences.[20] The MOBCAL trajectory

DOI: 10.1021/acs.analchem.7b02932
Anal. Chem. XXXX, XXX, XXX−XXX

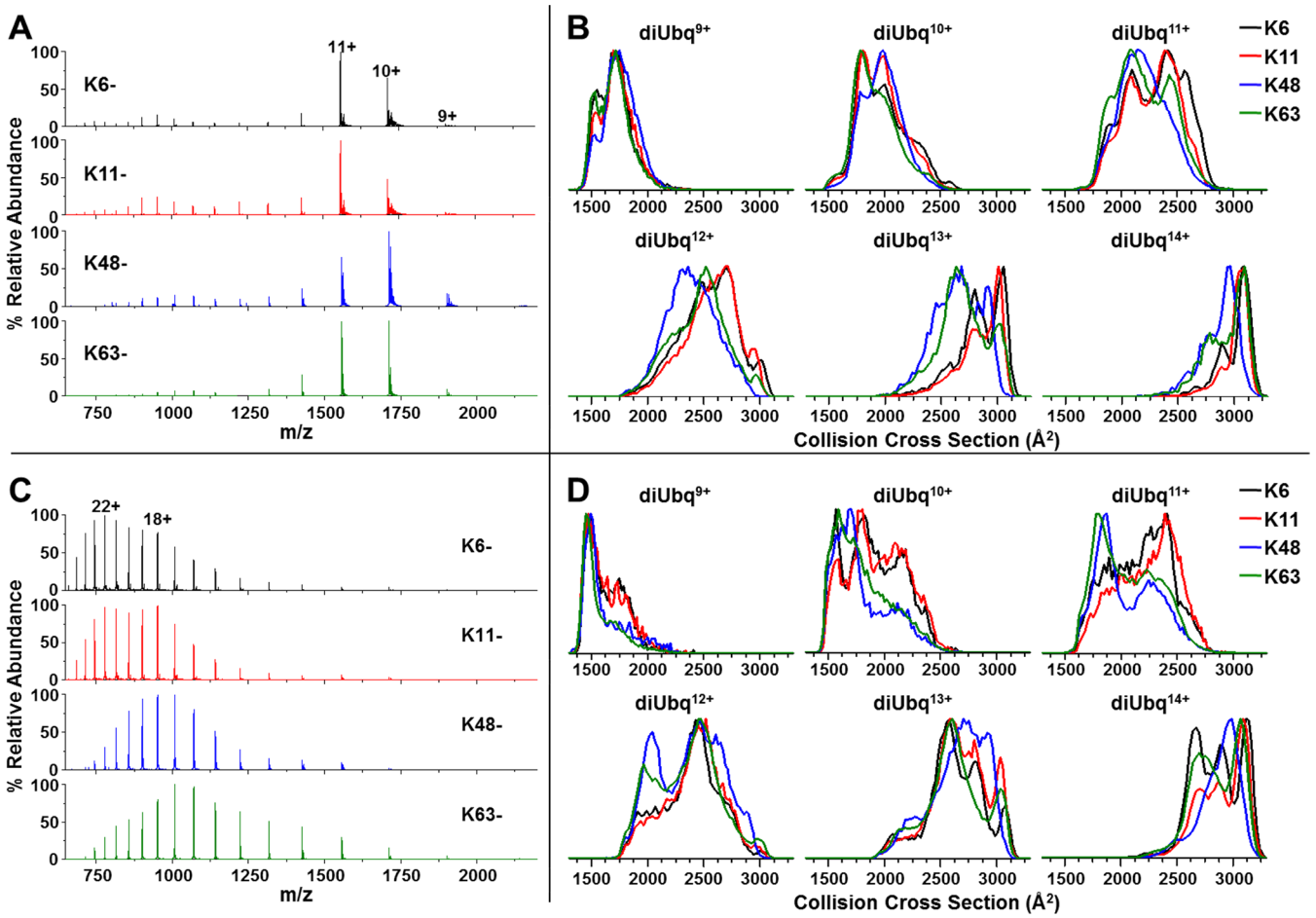

Figure 1. (A,C) Full mass spectra and (B,D) CCS profiles acquired with minimal collsional activation for K6 (black)-, K11 (red)-, K48 (blue)-, and K63 (green)-linked diUbq acquired from (A,B) 99.9% water and 0.1% formic acid and (C,D) 50% methanol, 49.9% water, and 0.1% formic acid. Select charge states are labeled.

method was used to calculate theoretical CCS values from PDB files.[66,67]

RESULTS AND DISCUSSION

Charge-Induced Unfolding of DiUbq Ions. Figure 1 shows the full ESI-IM-MS mass spectra and CCS profiles acquired using instrument conditions that minimize collisional activation to preserve more native-like conformations[30] for K6-, K11-, K48-, and K63-linked diUbq acquired from 99.9% water and 0.1% formic acid. All ions discussed throughout this Article are charged only through differences in protonation; therefore, ions of the form $[\text{diUbq} + n\text{H}]^{n+}$ will be abbreviated as diUbq^{n+} for the remainder of the text. The charge state distributions observed of all four diUbq types from water/formic acid exhibit a narrow distribution of high abundance, low charge states (10−11+) and a broad distribution of low abundance, high charge states (13−25+). Note, however, that the abundances of each charge state differ for the different linkage sites of diUbq.

It has been shown that ESI−MS charge state distributions can be correlated to protein conformational preference.[68,69] That is, the charge state of a protein in the ESI mass spectrum is related to the solvent accessible surface area (SASA), as related to solvent exposure of basic/acidic residues and the presence of intramolecular interactions.[70−72] Under acidic conditions, monoUbq produces a narrow distribution of low charge states centered around the Ubq^{7+} ion and a low abundance of higher charge states, which suggests retention of native-like states, but the observed higher charge states, IMS CCS profiles, and radical-directed fragmentation experiments provide evidence for a small population of unfolded conformers.[26,73] The mass spectra acquired for all four diUbq linkage types from water/formic acid illustrate similar behavior, suggesting retention of native-like conformations (Figure 1A). Note, however, that the abundances of the charge states differ for the different linkage sites of diUbq, suggesting differing exposure of basic residues due to differences in conformation or intramolecular bonding. K63- and K48-linked diUbq in particular populate on average lower charge states than do K6- and K11-linked diUbq. This finding is consistent with results reported by Lee et al.; complexation of the K6 or K11 side-chains of monoUbq by host−guest chemistry destabilizes the native conformation and induces preference for higher charge states.[74]

The CCS profiles of diUbq ions (Figure 1B) indicate sensitivity to the charge state of the ion and to the linkage site when higher charge state ions are sampled; however, the CCS profiles of diUbq^{9+} ions are relatively narrow for all linkage types and suggest two conformational families: ∼1500 and 1750 Å^2. The larger of the two CCS values is similar to the theoretical CCS values of K48-linked diUbq reported previously (1780 Å^2 for the "closed" conformation PDB 2PEA, 1816 Å^2 for the "open" conformation PDB 3NS8),[64] suggesting that these ion populations retain much of the solution-phase structure.

DOI: 10.1021/acs.analchem.7b02932
Anal. Chem. XXXX, XXX, XXX−XXX

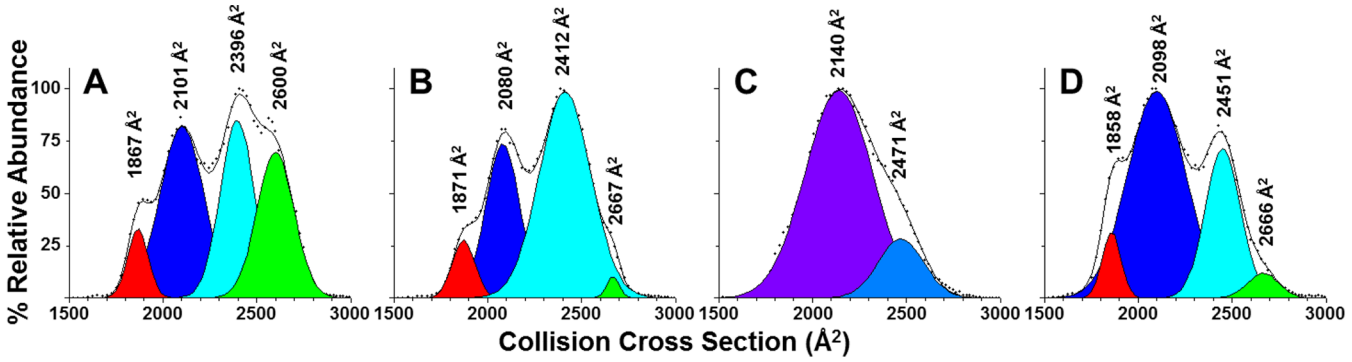

Figure 2. Deconvolution of (A) K6-, (B) K11-, (C) K48-, and (D) K63-diUbq^{11+} CCS profiles. The raw data are represented as data points, the cumulative fit is represented as a black line, and the fitted peaks are filled such that like colors depict fit peaks.

Furthermore, K63-diUbq^{9+} is not observed populating an open conformation (calculated CCS of 2086 Å^2, PDB 2JF5). The smaller of the two CCS values was previously defined as that of acid-induced molten globule conformations through comparison with CCS profiles acquired from buffered solution.[64] The MOBCAL calculated theoretical CCS values for diUbq structures reported in the PDB are 1829 and 1845 Å^2 for K6- and K11-linked diUbq, respectively (PDB structures 2XK5 and 2XEW, respectively). The percent difference between these structures and those reported for K48-linked diUbq is approximately 3%; consequently, the inability to differentiate K6-, K11-, and K48-linked conformations using IM-MS is unsurprising.

The CCS profiles of the higher charge states shift to larger CCS values, suggesting increasing degrees of gas-phase unfolding due to their increasing Coulombic repulsion and lab-frame collision energies. The diUbq^{10+} and diUbq^{11+} ions of all four linkage types exhibit broad distributions with distinct conformational populations. Peak deconvolution of diUbq^{11+} ion CCS profiles is shown in Figure 2. The CCS profiles of K6-, K11-, and K63-diUbq^{11+} ions each demonstrate four broad conformational families where CCS centroid values vary less than 3% for each linkage type; the primary difference between the three linkage types is the relative abundance of the different conformational families. The K48-diUbq^{11+} distributions are better represented with a fit that involves two more broadened peaks with CCS centroid values shifted relative to the other linkage types. The CCS profiles of diUbq^{12+} ions are still broad, but relatively featureless; however, the degree of unfolding varies relative to linkage site. The majority of K6- and K11-diUbq^{13+} ions populate a narrow distribution of extended conformers, whereas the K48- and K63-diUbq^{13+} ions retain a broad distribution of ions with largely intermediate CCS values. diUbq^{14+} ions of all linkage types populate primarily narrow CCS distributions of extended conformers that likely represent gas-phase equilibrium conformations.

Solvent-Induced Denaturation of DiUbq. Upon addition of >40% methanol to acidic solution (pH ≈ 2), monoUbq is known to populate the "denatured" A-state conformation, wherein part of the N-terminal portion of the β-sheet is retained, but the rest of the structure is in a flexible conformation with a high degree of α-helical character.[47,75−77] The mass spectra acquired of monoUbq exhibit a broad distribution of high charge state ions consistent with the increased SASA.[24,26] The calculated CCS for the A-state of monoUbq is larger than that of the N-state, and experimental CCS profiles of monoUbq are consistently shifted to larger CCS when acquired from methanolic solutions with low pH.[26,29,78] Figure 1C and D shows the full ESI−MS mass spectra and CCS profiles, respectively, for K6-, K11-, K48-, and K63-linked diUbq acquired from 49.9% water, 50% methanol, and 0.1% formic acid. The ESI mass spectra of diUbq acquired from these denaturing conditions indicate a broad distribution of high charge states, similarly suggesting increased SASA, but the spectra differ for each linkage type. K48-linked diUbq exhibits a more narrow charge state distribution centered at the 18+ charge state. K6- and K11-linked diUbq exhibit bimodal charge state distributions centered on the 18+ and 22+ charge states. K63-linked diUbq exhibits an even broader charge state distribution, possibly trimodal, centered at the 17+ charge state. The presence of multiple broad distributions of high charge states for K6-, K11-, and K63-linked diUbq from the denaturing solution conditions suggests a high degree of conformational heterogeneity in solution. The distribution of charge states for K6- and K11-linked diUbq is significantly higher than those observed for K48- and K63-linked diUbq indicative of further increased SASA.

The CCS profiles of low charge state diUbq ions of all four linkage types acquired from acidic 50% methanol solution (Figure 1D) suggest that the ions adopt more compact conformers than those observed from acidic aqueous solution. This observed preference for compact conformers is contrary to the larger CCS observed for monoUbq under similar conditions, suggesting the collapse of the ion's tertiary structure. Interestingly, the CCS of the more compact diUbq^{9+} conformer observed from denaturing conditions is similar to that of the ∼1500 Å^2 diUbq^{9+} conformer previously attributed to an acid-induced molten globule conformation. Thus, we attribute the more compact conformer observed from denaturing conditions to a collapsed, partially folded conformation likely possessing a high degree of α-helical character or a molten globule-type conformation.

Gas-Phase Unfolding of DiUbq Ions. CIU is similar to gas-phase annealing; collisional activation (unfolding) is followed by collisional cooling (thermalization) prior to IM separation; consequently, CIU provides information concerning the gas-phase potential energy surface en route to the gas-phase equilibrium conformation as defined by their noncovalent interactions. CCS profiles for the four linkage types of diUbq were acquired with increasing collisional activation and assembled into heat maps, or CIU fingerprints, to illustrate the changing conformational preference of the protein en route to the gas-phase equilibrium conformation (Figure 3; see Figures S1−4 for raw CCS profiles used to assemble CIU plots). Overall, the CIU fingerprints of each linkage type acquired under N-state

DOI: 10.1021/acs.analchem.7b02932
Anal. Chem. XXXX, XXX, XXX−XXX

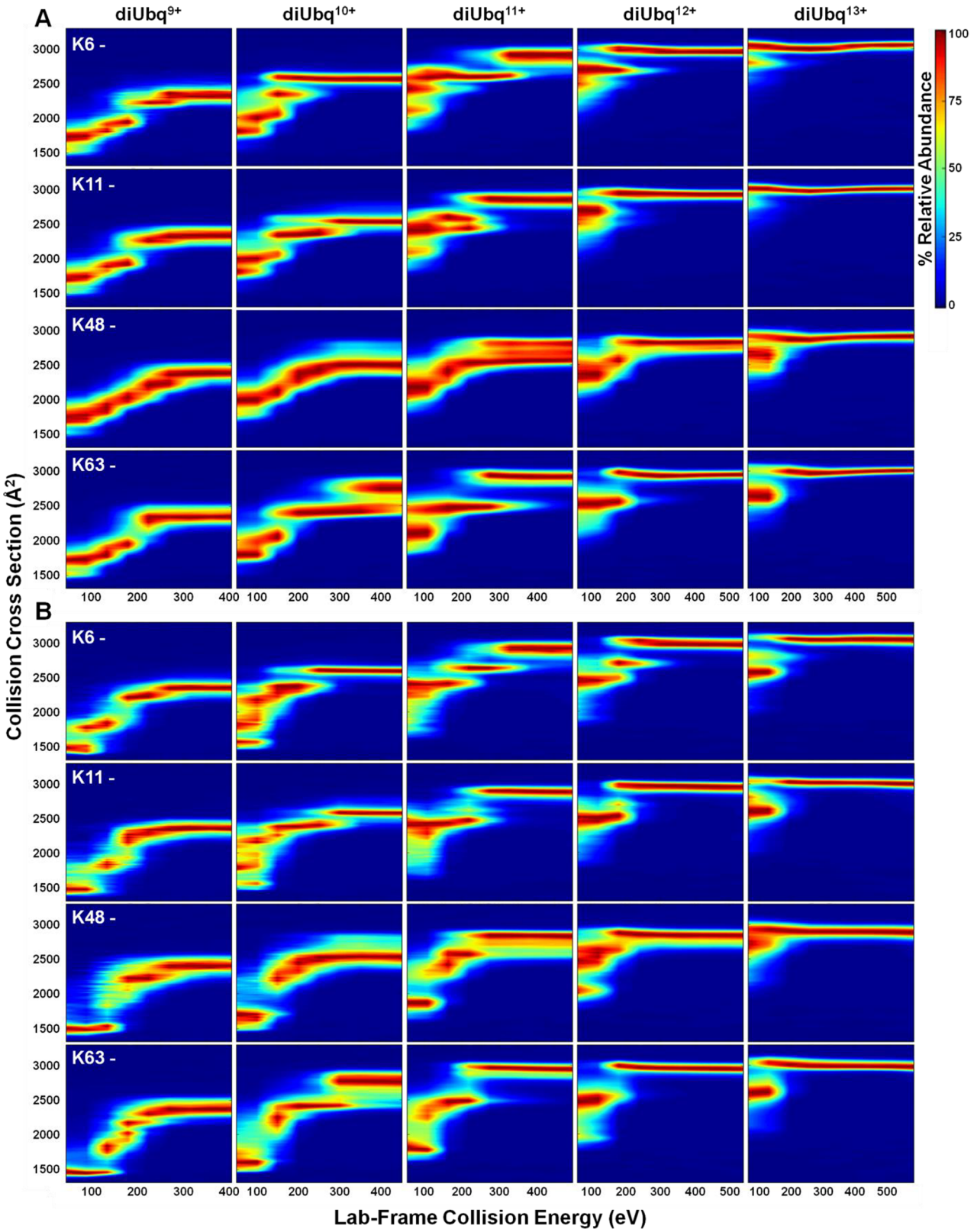

Figure 3. CIU heat maps for K6-, K11-, K48-, and K63-linked diUbq (top to bottom) with 9−13+ charge states (left to right) acquired from (A) 99.9% water and 0.1% formic acid and (B) 49.9% water, 50% methanol, and 0.1% formic acid.

conditions differ noticeably from one another (Figure 3A). These differences are highlighted by the use of difference plots (Figures S5−8) and calculated RMSD values (summarized in Figure 4).

The RMSD values and difference plots indicate that the CIU of K48-linked diUbq differs most significantly from the other linkage types due to the absence of distinct unfolding intermediates and generally more compact extended conformers

DOI: 10.1021/acs.analchem.7b02932
Anal. Chem. XXXX, XXX, XXX−XXX

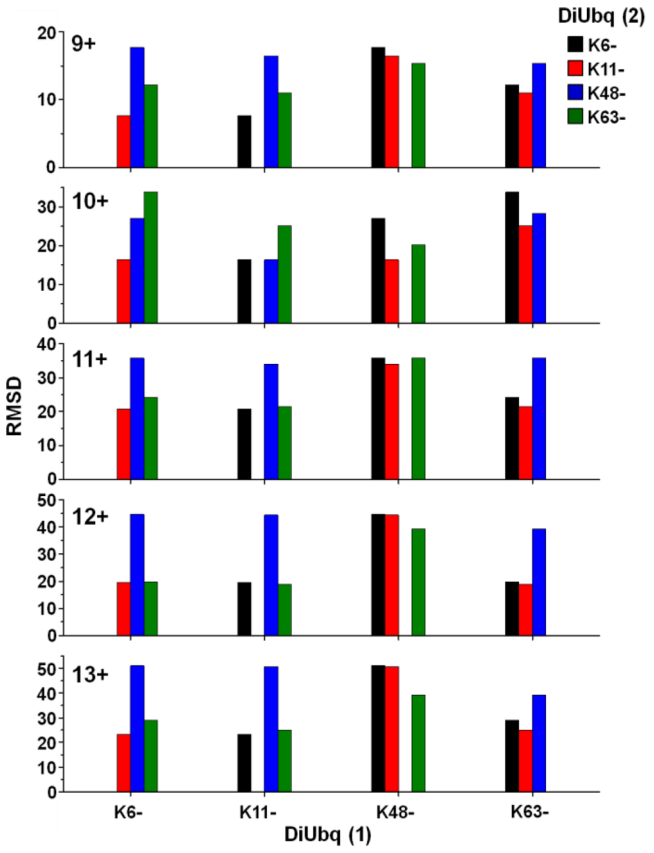

Figure 4. Root-mean-square deviation values calculated for two CIU heats maps, DiUbq (1) minus DiUbq (2). For example, the blue bar in the 9+, K11 cluster represents the RMSD value for K11- and K48-diUbq^{9+} ion CIU profiles.

than those observed of the other linkage types. Specifically, the CIU fingerprints of lower charge states of K48-linked diUbq indicate that the ions undergo gradual unfolding until the late stages of the unfolding process, whereas the CIU profiles of K6-, K11-, and K63-linked diUbq indicate interconversion between distinct intermediate conformers. Furthermore, K48-diUbq^{10+}, diUbq^{11+}, and diUbq^{12+} populate three distinct extended conformers, most apparent of the 11+ ion, which remain stable until fragmentation. An exception to the exclusively large RMSD values observed for K48-linked diUbq ions are the large RMSD values observed for K63-diUbq^{10+} ions due to large differences in the late stages of unfolding. The most extended conformer of K63-[diUbq +10H]$^{10+}$ is observed only after a high degree of collisional activation and in much higher abundance than a similar conformer observed of K11- and K48-diUbq^{10+} (see Figure S1 for details). The distinct unfolding intermediates of K6-, K11-, and K63-linked diUbq ions exhibit CCS values similar to one another but with differing stabilities. This suggests that these ions populate similar conformational populations en route to the gas-phase equilibrium structure. This observation is consistent with that reported by Eschweiler et al. wherein collisional activation of albumin homologues populates very similar conformational unfolding intermediates, but the stability of each varied with differing 1° structure.[79]

The CIU fingerprints of the diUbq ions acquired from denaturing conditions bear striking differences from those acquired from "native" conditions, but also interesting similarities in the late stages of unfolding (Figure 3B). These observations are demonstrated most vividly by difference plots (see Figure 5 for diUbq^{9+} and diUbq^{13+} ions; see Figure S9 for all charge states). As discussed previously, the CCS profiles of the "denatured" diUbq ions are shifted to lower CCS than those acquired from "native" conditions. Interestingly, the CIU profiles of K48-linked diUbq ions acquired from the denaturing conditions exhibit the distinct unfolding intermediates observed of the other linkage types in "native" conditions. This suggests that the gradual unfolding observed previously is characteristic of the native K48-linked diUbq solution-phase structure. The CCS profiles of all diUbq linkage types acquired from "native" and "denatured" conditions converge to similar conformational families upon application of high collision energies. This provides an indication as to when all aspects of the solution-phase "conformational memory" are lost in favor of gas-phase equilibrium conformations. The CIU profiles of K48-linked diUbq acquired from both solution conditions are increasingly similar with increasing charge state. Oddly, the gas-phase equilibrium conformers of the higher charge states of K6-, K11-, and K63-linked diUbq ions acquired from the denaturing solution conditions adopt a smaller CCS than those acquired from more native conditions.

Shi et al. have previously reported that the relative abundances of different extended conformers of monoUbq are influenced by the addition of methanol.[78,80] The addition of methanol appears to have a similar influence on the conformational preference of extended K48-diUbq^{11+} conformers; specifically, the more compact of the extended conformers is less preferred. The most likely explanation for these differences in gas-phase equilibrium conformation would be differences in charge location as defined during the ESI process. The residues K6, K11, and K63 are located near the N- and C-termini, meaning fully extended conformations of diUbq covalently linked through those residues are nearly linear. Contrarily, K48 is located near the center of the sequence, meaning a fully extended conformation of K48-linked diUbq would resemble a "T" shape. Consequently, differences in charge location would more likely result in multiple extended conformations upon collisional activation.

Unraveling Differences in Noncovalent Intramolecular DiUbq Interactions. The effect of collisional activation on the conformation of multidomain proteins is oft-debated, mainly due to observed asymmetric charge partitioning between dissociated subunits. Wysocki et al. suggest that asymmetric charge partitioning is evidence that collisional activation results in subunit unfolding,[12] whereas Loo and Loo posit that charge state differences may be a function of salt bridge rearrangement such that collisional activation may still result in disassociation of the subunit interface.[81] Eschweiler et al. have recently used chemical probes to monitor the sequential unfolding of albumin domains; distinct unfolding intermediate transitions were correlated with the loss of subunit bound ligands, suggesting sequential subunit unfolding upon collisional activation.[79] We have previously suggested that the subunit interface of K48-linked diUbq ions persists until the late stages of unfolding via comparisons with noncovalent Ubq dimer unfolding and disassociation energies.[64]

The specific gas-phase unfolding pathway of monoUbq has been previously discussed by Skinner et al. using electron capture dissociation experimental results[82] and by Chen et al. using molecular dynamics simulations.[30] The N- and C-terminal β-strands located in the center of the β sheet structure are in particular only weakly stabilized in the gas phase, meaning collisional activation likely results first in the loss of the five-stranded β-sheet structure. This "weakness" provides much

DOI: 10.1021/acs.analchem.7b02932
Anal. Chem. XXXX, XXX, XXX−XXX

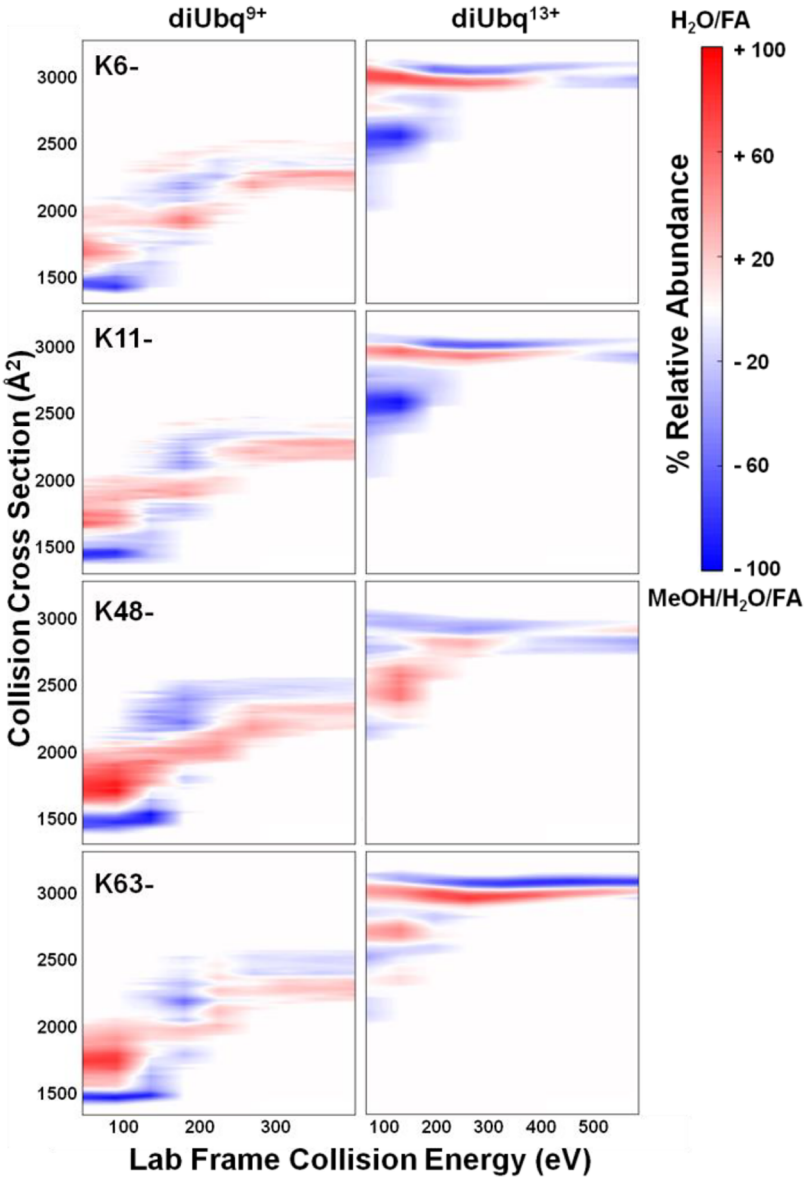

Figure 5. Difference plots calculated using CIUSuite, where the CIU heat maps of diUbq^{9+} (left) and diUbq^{13+} (right) ions acquired from 50% methanol/49.9% water/0.1% formic acid (blue) are subtracted from the CIU profiles acquired from 99.9% water/0.1% formic acid (red). Note that the difference plots for all other charge states can be found in the Supporting Information.

insight into the unfolding patterns observed of the diUbq ions. The residues of the I44 patch are located on three individual β-strands, including both the N- and the C-terminal; consequently, any subunit interfacing with the other via the I44 patch would benefit from significant stabilization of the β-sheet. The residues from the I36 patch are located on the C-terminal β-strand, but not on the N-terminal β-strand, such that participation of the I36 patch in the subunit interface will have no effect on the stability of the β-sheet. K48-linked diUbq preferentially forms I44/I44 interfacial interactions unless Coulombic repulsion of R42 and R72 in close proximity to the I44 hydrophobic faces induces the preference for electrostatic interfacial interactions.[32,50] On the basis of the aforementioned possible influence of I44 patch interactions on the stability of each subunit, it would be expected that an I44/I44 interface would impart dramatic stabilization of both Ubq subunits. We have previously reported that the unique gradual unfolding observed in the CIU fingerprints of K48-diUbq^{9+} and diUbq^{11+} is indicative of I44/I44 hydrophobic interfacial interactions; furthermore, the R42 and R72 residues play an important role in stabilization of the subunit interface.[64,83] The observed gradual unfolding of the additional charge states further supports the differentiation of the K48-linked diUbq subunit interface as unique from that observed of other linkage sites.

As noted repeatedly, K6-, K11-, and K63-linked diUbq ions demonstrate substantial CIU similarity. With increasing collision energy, each undergoes conversion between distinct intermediates en route to the most extended conformations. As discussed previously, K63-linked diUbq is stabilized exclusively by electrostatic interactions; consequently, the most obvious conclusion that can be drawn from the similarity between the CIU fingerprints of K6-, K11-, and K63 linked diUbq is that the lower charge states of all three linkage types exhibit electrostatic interfacial interactions. The gas-phase stability of an electrostatic interface would depend greatly on the number of salt bridges and ionic hydrogen bonds formed between the subunits resulting in

DOI: 10.1021/acs.analchem.7b02932
Anal. Chem. XXXX, XXX, XXX−XXX

differing stabilities, dependent on linkage site and charge state. Thus, differences in the unfolding pathway could be the product of different available electrostatic interactions induced by the changing proximities of charge groups induced by the covalent linkage site. A solution-phase structure of K11-linked diUbq is reported that demonstrates electrostatic interfacial stabilization;[55] however, another reports an I36/I36 interface.[53]

Both K6- and K11-linked diUbq have reported conformations utilizing the I36 hydrophobic patch for interfacial interaction. The crystal structure of K6-linked diUbq, specifically, was reported to exhibit an I36/I44 interface, where the I36 patch of the proximal Ubq subunit interacts with the I44 patch of the distal Ubq subunit. Thus, it would be expected that the proximal subunit would unfold upon collisional activation due to the instability of its β-sheet, followed by the unfolding of the distal subunit. Both subunits of K11-linked diUbq would be expected to unfold upon collisional activation due to the preference for an I36/I36 interface. As such, K6- and K11-linked diUbq would be expected to demonstrate significantly different unfolding pathways. Consequently, the resemblance between the K6-, K11-, and K63-linked diUbq CIU fingerprints could be attributed to two scenarios: all three adopt electrostatic interfacial interactions, or the unfolding pathway of interfacial interactions involving I36 is similar to that demonstrated by K63-linked diUbq ions.

As noted above, the intermediate charge states (i.e., 10+ and 11+) of K6-, K11-, and K63-linked diUbq exhibit low energy CCS profiles, suggesting similar conformational preferences (see Figure 2). Upon collision activation, these diUbq ions transition through similar conformational families en route to gas-phase equilibrium conformers. Furthermore, through comparison of CIU profiles for diUbq ions acquired from native and denaturing conditions, the collision energy after which gas-phase conformers are populated is known; that is, any unfolding intermediates observed prior to forming gas-phase conformers are characteristic of a solution-phase structure. Upon collisional activation of K6- and K11-linked diUbq^{10+} and diUbq^{11+} ions, each adopt two distinct unfolding intermediates, labeled as I^E (CCS $\approx$ 2400 Å^2) and I^H (CCS $\approx$ 2600 Å^2) in Figure 6. A relatively small population of K6-linked diUbq^{10+} and diUbq^{11+} ions transition through the more compact unfolding intermediate (I^E). Interestingly, the I^H unfolding intermediate is not observed in the unfolding pathways of K63-linked diUbq^{10+} and diUbq^{11+} ions. This suggests that I^E unfolding intermediates may be characteristic of diUbq ions exhibiting purely electrostatic interfacial interactions, whereas I^H unfolding intermediates may be characteristic of diUbq ions exhibiting alternative interfacial interactions, such as hydrophobic interfacial interactions via the I36 hydrophobic patch. This is consistent with the aforementioned two distinct structures previously reported for K11-linked diUbq ions exhibiting either I36/I36 hydrophobic interactions or electrostatic interfacial interactions;[41,53−55] a relatively high abundance of both unfolding intermediates is observed upon CIU of K11-linked diUbq^{10+} and diUbq^{11+} ions, suggesting a mixture of two conformational populations with distinctly different unfolding pathways. However, these data are the first to suggest that K6-linked diUbq may adopt a mixture of conformers wherein a relatively small population may exhibit electrostatic interfacial interactions.

CONCLUSIONS

Here, we demonstrate the use of ESI-IM-MS and CIU to probe the differences in noncovalent intramolecular interactions

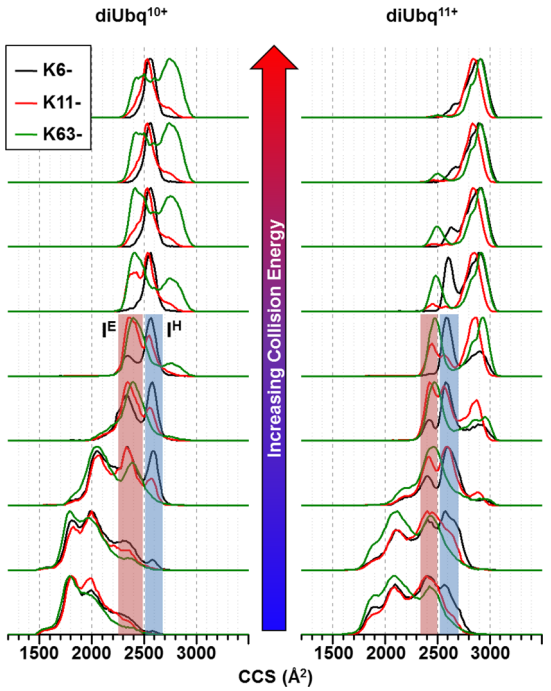

Figure 6. Stacked CCS profiles after varying degrees of collisional activation (collision voltage was 5−45 V in 5 V increments) for the 10+ (left) and 11+ (right) charge states of protonated K6 (black)-, K11 (red)-, and K63 (green)-linked diUbq acquired from 99.9% water/0.1% formic acid. Unfolding intermediate peaks with similar CCS values are denoted as I^E (shaded red) and I^H (shaded blue). Note that shading ends at the point where the CCS profiles no longer differ from those acquired from denaturing conditions.

responsible for the conformational heterogeneity of the most abundant covalent linkage types of diUbq. The ESI mass spectra of each linkage type suggest that the ions sampled are "native-like" in conformation. Furthermore, the CCS profiles of diUbq^{9+} ions are centered on a CCS similar to theoretical CCS values calculated from PDB structures; however, because the CCS of the "native-like" conformers are within the error of the IMS experiment, solution-phase and gas-phase denaturation provides the additional information necessary to differentiate the conformational differences induced by the covalent linkage site.

Unfolding upon removal of solvent, driven by Coulomb repulsion as well as collisional activation, shows that K48-linked diUbq is unique in its conformational preference and gas-phase stability. We posit that this difference is the result of added stabilization of the β-sheet structure induced by I44/I44 interfacial interactions. Solvent-induced denaturation disrupts the hydrophobic patches apparent in the native fold of the subunits and reduces the burial of hydrophobic side chains within the interior of the structure; therefore, any remaining noncovalent interactions are unlikely to involve hydrophobic interactions. Upon solvent-induced denaturation, the gradual unfolding observed of K48-linked diUbq ions is no longer observed in favor of distinct unfolding intermediates.

Reported K6- and K11-linked diUbq structures suggest interfacial interactions involving either the I36 patch or electrostatic interactions. Because of the inaccessibility of hydrophobic patch interactions induced by covalent linkage through K63, electrostatic interactions are preferred for K63-linked diUbq interfacial interactions. K6-, K11-, and K63-linked diUbq ions demonstrate very similar unfolding pathways

DOI: 10.1021/acs.analchem.7b02932
Anal. Chem. XXXX, XXX, XXX−XXX

including distinct unfolding intermediate conformers very similar in CCSs but differing in relative stabilities. Therefore, the similarities between the K6-, K11-, and K63-linked diUbq CIU profiles could be indicative that K6- and K11-linked diUbq ions also adopt primarily electrostatic interfacial interactions. However, interfacial interactions involving the I36 patch would not lead to substantial stabilization of the weakly bound β-sheet structure, and thus such structures may unfold in a manner similar to those of K63-linked diUbq ions. Further comparison of CIU intermediates observed of K6-, K11-, and K63-linked diUbq ions suggests that both K6- and K11-linked diUbq adopt a heterogeneous mixture of conformers exhibiting electrostatic interfacial interactions or hydrophobic interfacial interactions involving the I36 hydrophobic patch. Overall, we have shown that ESI-IM-MS and CIU can provide a wealth of information concerning the noncovalent interactions stabilizing the conformational preference of diUbq ions; however, as with many IMS experiments, molecular dynamics simulations or solution-phase NMR would be excellent complementary techniques to provide more detailed atomistic information. Furthermore, the observed unique CIU fingerprints may provide the ability to perform fast screening of the covalent-linkage site of Ubq isomers and possibly characterization of longer, branched, or heterogeneous polyUbq, a heretofore challenging analytical problem due to the complexity and diversity of the Ubq code.

As noted in the introduction, covalent linkage between Ubq subunits is observed for all eight amino groups, each with unique functions. In addition to the four most common linkage types discussed here, covalent linkage between Ubq subunits is observed via the N-terminus (M1-linked or linear diUbq) and the three other lysine side chains (K27, K29, and K33).[31,37] Casteñada et al. have performed extensive analyses using NMR of the noncanonical linkage types of diUbq, reporting that K27-, K29-, and K33-linked diUbq exhibit little subunit interfacial interactions, and, most notably, hydrophobic patch interfacial interactions were not observed.[58] Furthermore, Casteñada et al. report that K29-linked diUbq adopts the most heterogeneous distribution of conformers and the isopeptide linkage of K27-linked diUbq is uniquely solvent inaccessible.[58] However, Kristariyanto et al. report a crystal structure for K33-linked diUbq demonstrating I36/I36 interfacial interactions[84] and a crystal structure for K29-linked diUbq with polar interfacial interactions.[85] Only recently has a quasi-racemic X-ray crystal structure of K27-linked diUbq been reported confirming the burial of the isopeptide linkage and absence of hydrophobic interfacial interactions, but suggesting a more compact conformer preference.[86] Linear diUbq reportedly adopts an open conformation nearly equivalent to that of K63-linked diUbq,[87] but a closed conformation of linear diUbq has yet to be reported. Overall, the conformational preferences of the noncanonical linkage types of diUbq are much less resolved and oft debated than those of the more canonical K48- and K63-linked diUbq; as such, CIU could provide invaluable information concerning the structural propensities of these alternative linkage types of diUbq and differentiation of heterogeneous conformer populations.

■ ASSOCIATED CONTENT

Supporting Information

The Supporting Information is available free of charge on the ACS Publications website at DOI: 10.1021/acs.analchem.7b02932.

Individual CCS profiles compiled into CIU plots; difference plots; and calculated RMSD values (PDF)

■ AUTHOR INFORMATION

Corresponding Author

*E-mail: russell@chem.tamu.edu.

ORCID

David E. Clemmer: 0000-0003-4039-1360

David H. Russell: 0000-0003-0830-3914

Notes

The authors declare no competing financial interest.

■ ACKNOWLEDGMENTS

Theoretical CCS values were calculated by Dr. Doyong Kim. This research was supported by the U.S. Department of Energy, Division of Chemical Sciences, Basic Energy Science (DE-FG02-04ER15520).

■ REFERENCES

(1) Bork, P.; Jensen, L. J.; Von Mering, C.; Ramani, A. K.; Lee, I.; Marcotte, E. M. *Curr. Opin. Struct. Biol.* **2004**, *14*, 292−299.

(2) Scarff, C.; Thalassinos, K.; Hilton, G.; Scrivens, J. *Rapid Commun. Mass Spectrom.* **2008**, *22*, 3297−3304.

(3) Fernandez-Lima, F. A.; Wei, H.; Gao, Y. Q.; Russell, D. H. *J. Phys. Chem. A* **2009**, *113*, 8221−8234.

(4) Jurneczko, E.; Barran, P. E. *Analyst* **2011**, *136*, 20−28.

(5) Konermann, L.; Vahidi, S.; Sowole, M. a. *Anal. Chem.* **2014**, *86*, 213−232.

(6) Ho, Y.; Gruhler, A.; Heilbut, A.; Bader, G. D.; Moore, L.; Adams, S.-L.; Millar, A.; Taylor, P.; Bennett, K.; Boutilier, K.; Yang, L.; Wolting, C.; Donaldson, I.; Schandorff, S.; Shewnarane, J.; Vo, M.; Taggart, J.; Goudreault, M.; Muskat, B.; Alfarano, C.; et al. *Nature* **2002**, *415*, 180−183.

(7) Krogan, N. J.; Cagney, G.; Yu, H.; Zhong, G.; Guo, X.; Ignatchenko, A.; Li, J.; Pu, S.; Datta, N.; Tikuisis, A. P.; Punna, T.; Peregrín-Alvarez, J. M.; Shales, M.; Zhang, X.; Davey, M.; Robinson, M. D.; Paccanaro, A.; Bray, J. E.; Sheung, A.; Beattie, B.; et al. *Nature* **2006**, *440*, 637−643.

(8) Taverner, T.; Hernández, H.; Sharon, M.; Ruotolo, B. T.; Matak-Vinković, D.; Devos, D.; Russell, R. B.; Robinson, C. V. *Acc. Chem. Res.* **2008**, *41*, 617−627.

(9) Heck, A. J. R. *Nat. Methods* **2008**, *5*, 927−933.

(10) Uetrecht, C.; Rose, R. J.; van Duijn, E.; Lorenzen, K.; Heck, A. J. R. *Chem. Soc. Rev.* **2010**, *39*, 1633−1655.

(11) Laganowsky, A.; Reading, E.; Hopper, J. T. S.; Robinson, C. V. *Nat. Protoc.* **2013**, *8*, 639−651.

(12) Wysocki, V. H.; Jones, C. M.; Galhena, A. S.; Blackwell, A. E. *J. Am. Soc. Mass Spectrom.* **2008**, *19*, 903−913.

(13) Zhou, M.; Jones, C. M.; Wysocki, V. H. *Anal. Chem.* **2013**, *85*, 8262−8267.

(14) Zhong, Y.; Han, L.; Ruotolo, B. T. *Angew. Chem., Int. Ed.* **2014**, *53*, 9209−9212.

(15) Hopper, J. T. S.; Oldham, N. J. *J. Am. Soc. Mass Spectrom.* **2009**, *20*, 1851−1858.

(16) Freeke, J.; Robinson, C. V.; Ruotolo, B. T. *Int. J. Mass Spectrom.* **2010**, *298*, 91−98.

(17) Cubrilovic, D.; Biela, A.; Sielaff, F.; Steinmetzer, T.; Klebe, G.; Zenobi, R. *J. Am. Soc. Mass Spectrom.* **2012**, *23*, 1768−1777.

(18) Laganowsky, A.; Reading, E.; Allison, T. M.; Ulmschneider, M. B.; Degiacomi, M. T.; Baldwin, A. J.; Robinson, C. V. *Nature* **2014**, *510*, 172−175.

(19) Liu, J.; Konermann, L. *J. Am. Soc. Mass Spectrom.* **2014**, *25*, 595−603.

(20) Eschweiler, J. D.; Rabuck-Gibbons, J. N.; Tian, Y.; Ruotolo, B. T. *Anal. Chem.* **2015**, *87*, 11516−11522.

DOI: 10.1021/acs.analchem.7b02932
Anal. Chem. XXXX, XXX, XXX−XXX

(21) Wagner, N. D.; Kim, D.; Russell, D. H. *Anal. Chem.* **2016**, *88*, 5934−5940.
(22) Vijay-Kumar, S.; Bugg, C. E.; Wilkinson, K. D.; Cook, W. J. *Proc. Natl. Acad. Sci. U. S. A.* **1985**, *82*, 3582−3585.
(23) Brutscher, B.; Bruschweiler, R.; Ernst, R. R. *Biochemistry* **1997**, *36*, 13043−13053.
(24) Babu, K. R.; Moradian, A.; Douglas, D. J. *J. Am. Soc. Mass Spectrom.* **2001**, *12*, 317−328.
(25) Jackson, S. E. *Org. Biomol. Chem.* **2006**, *4*, 1845−1853.
(26) Wyttenbach, T.; Bowers, M. T. *J. Phys. Chem. B* **2011**, *115*, 12266−12275.
(27) Koeniger, S. L.; Clemmer, D. E. *J. Am. Soc. Mass Spectrom.* **2007**, *18*, 322−331.
(28) Segev, E.; Wyttenbach, T.; Bowers, M. T.; Gerber, R. B. *Phys. Chem. Chem. Phys.* **2008**, *10*, 3077−3082.
(29) Shi, H.; Atlasevich, N.; Merenbloom, S. I.; Clemmer, D. E. *J. Am. Soc. Mass Spectrom.* **2014**, *25*, 21−26.
(30) Chen, S. H.; Russell, D. H. *J. Am. Soc. Mass Spectrom.* **2015**, *26*, 1433.
(31) Avram, H. In *Ubiquitin and the Biology of the Cell*; Peters, J.-M., Harris, J. R., Finley, D., Eds.; Springer: U.S., 1998.
(32) Varadan, R.; Walker, O.; Pickart, C.; Fushman, D. *J. Mol. Biol.* **2002**, *324*, 637−647.
(33) Varadan, R.; Assfalg, M.; Haririnia, A.; Raasi, S.; Pickart, C.; Fushman, D. *J. Biol. Chem.* **2004**, *279*, 7055−7063.
(34) Fushman, D.; Wilkinson, K. D. *F1000 Biol. Rep.* **2011**, *3*, 26.
(35) Komander, D.; Rape, M. *Annu. Rev. Biochem.* **2012**, *81*, 203−229.
(36) Ye, Y.; Blaser, G.; Horrocks, M. H.; Ruedas-Rama, M. J.; Ibrahim, S.; Zhukov, A. A.; Orte, A.; Klenerman, D.; Jackson, S. E.; Komander, D. *Nature* **2012**, *492*, 266−270.
(37) Kleiger, G.; Mayor, T. *Trends Cell Biol.* **2014**, *24*, 352−359.
(38) Collins, C. A.; Brown, E. J. *Trends Cell Biol.* **2010**, *20*, 205−213.
(39) Ross, C. A.; Pickart, C. M. *Trends Cell Biol.* **2004**, *14*, 703−711.
(40) Bennett, E. J.; Shaler, T. A.; Woodman, B.; Ryu, K. Y.; Zaitseva, T. S.; Becker, C. H.; Bates, G. P.; Schulman, H.; Kopito, R. R. *Nature* **2007**, *448*, 704−708.
(41) Wickliffe, K. E.; Williamson, A.; Meyer, H. J.; Kelly, A.; Rape, M. *Trends Cell Biol.* **2011**, *21*, 656−663.
(42) Bennett, E. J.; Harper, J. W. *Nat. Struct. Mol. Biol.* **2008**, *15*, 20−22.
(43) Chen, Z. J.; Sun, L. J. *Mol. Cell* **2009**, *33*, 275−286.
(44) Wertz, I. E.; Newton, K.; Seshasayee, D.; Kusam, S.; Lam, C.; Zhang, J.; Popovych, N.; Helgason, E.; Schoeffler, A.; Jeet, S.; Ramamoorthi, N.; Kategaya, L.; Newman, R. J.; Horikawa, K.; Dugger, D.; Sandoval, W.; Mukund, S.; Zindal, A.; Martin, F.; Quan, C.; et al. *Nature* **2015**, *528*, 370−375.
(45) Peisley, A.; Wu, B.; Xu, H.; Chen, Z. J.; Hur, S. *Nature* **2014**, *509*, 110−114.
(46) Hoeller, D.; Dikic, I. *Nature* **2009**, *458*, 438−444.
(47) Lenkinski, R. E.; Chen, D. M.; Glickson, J. D.; Goldstein, G. *Biochim. Biophys. Acta, Protein Struct.* **1977**, *494*, 126−130.
(48) Xu, P.; Duong, D. M.; Seyfried, N. T.; Cheng, D.; Xie, Y.; Robert, J.; Rush, J.; Hochstrasser, M.; Finley, D.; Peng, J. *Cell* **2009**, *137*, 133−145.
(49) Hirano, T.; Serve, O.; Yagi-Utsumi, M.; Takemoto, E.; Hiromoto, T.; Satoh, T.; Mizushima, T.; Kato, K. *J. Biol. Chem.* **2011**, *286*, 37496−37502.
(50) Lai, M. Y.; Zhang, D.; Laronde-Leblanc, N.; Fushman, D. *Biochim. Biophys. Acta, Mol. Cell Res.* **2012**, *1823*, 2046−2056.
(51) Ryabov, Y.; Fushman, D. *Proteins: Struct., Funct., Genet.* **2006**, *63*, 787−796.
(52) Liu, Z.; Gong, Z.; Jiang, W. X.; Yang, J.; Zhu, W. K.; Guo, D. C.; Zhang, W. P.; Liu, M. L.; Tang, C. *eLife* **2015**, *4*, 1 DOI: 10.7554/eLife.05767.
(53) Matsumoto, M. L.; Wickliffe, K. E.; Dong, K. C.; Yu, C.; Bosanac, I.; Bustos, D.; Phu, L.; Kirkpatrick, D. S.; Hymowitz, S. G.; Rape, M.; Kelley, R. F.; Dixit, V. M. *Mol. Cell* **2010**, *39*, 477−484.
(54) Bremm, A.; Komander, D. *Trends Biochem. Sci.* **2011**, *36*, 355−363.
(55) Bremm, A.; Freund, S. M. V.; Komander, D. *Nat. Struct. Mol. Biol.* **2010**, *17*, 939−947.
(56) Virdee, S.; Ye, Y.; Nguyen, D. P.; Komander, D.; Chin, J. W. *Nat. Chem. Biol.* **2010**, *6*, 750−757.
(57) Fushman, D. *Structure* **2017**, *25*, 1−3.
(58) Castaneda, C. A.; Chaturvedi, A.; Camara, C. M.; Curtis, J. E.; Krueger, S.; Fushman, D. *Phys. Chem. Chem. Phys.* **2016**, *18*, 5771−5788.
(59) Editors, S. *Spectroscopy* **2015**, *30*, 38−41.
(60) Newton, K.; Matsumoto, M. L.; Wertz, I. E.; Kirkpatrick, D. S.; Lill, J. R.; Tan, J.; Dugger, D.; Gordon, N.; Sidhu, S. S.; Fellouse, F. A.; Komuves, L.; French, D. M.; Ferrando, R. E.; Lam, C.; Compaan, D.; Yu, C.; Bosanac, I.; Hymowitz, S. G.; Kelley, R. F.; Dixit, V. M. *Cell* **2008**, *134*, 668−678.
(61) Hospenthal, M. K.; Mevissen, T. E. T.; Komander, D. *Nat. Protoc.* **2015**, *10*, 349−361.
(62) Lee, A. E.; Castaneda, C. A.; Wang, Y.; Fushman, D.; Fenselau, C. *J. Mass Spectrom.* **2014**, *49*, 1272−1278.
(63) Xu, P.; Peng, J. *Anal. Chem.* **2008**, *80*, 3438−3444.
(64) Wagner, N. D.; Russell, D. H. *J. Am. Chem. Soc.* **2016**, *138*, 16588−16591.
(65) Ruotolo, B. T.; Benesch, J. L. P.; Sandercock, A. M.; Hyung, S.-J.; Robinson, C. V. *Nat. Protoc.* **2008**, *3*, 1139−1152.
(66) Mesleh, M. F.; Hunter, J. M.; Shvartsburg, A. A.; Schatz, G. C.; Jarrold, M. F. *J. Phys. Chem.* **1996**, *100*, 16082−16086.
(67) Shvartsburg, A. A.; Jarrold, M. F. *Chem. Phys. Lett.* **1996**, *261*, 86−91.
(68) Chowdhury, S. K.; Katta, V.; Chait, B. T. *J. Am. Chem. Soc.* **1990**, *112*, 9012−9013.
(69) Loo, J. A.; Loo, R. R. O.; Udseth, H. R.; Edmonds, C. G.; Smith, R. D. *Rapid Commun. Mass Spectrom.* **1991**, *5*, 101−105.
(70) Iavarone, a. T.; Jurchen, J. C.; Williams, E. R. *J. Am. Soc. Mass Spectrom.* **2000**, *11*, 976−985.
(71) Hall, Z.; Robinson, C. V. *J. Am. Soc. Mass Spectrom.* **2012**, *23*, 1161−1168.
(72) Hamdy, O. M.; Julian, R. R. *J. Am. Soc. Mass Spectrom.* **2012**, *23*, 1−6.
(73) Ly, T.; Julian, R. R. *J. Am. Chem. Soc.* **2010**, *132*, 8602−8609.
(74) Lee, J. W.; Heo, S. W.; Lee, S. J. C.; Ko, J. Y.; Kim, H.; Kim, H. I. *J. Am. Soc. Mass Spectrom.* **2013**, *24*, 21.
(75) Harding, M. M.; Williams, D. H.; Woolfson, D. N. *Biochemistry* **1990**, *30*, 3120−3128.
(76) Brutscher, B.; Bruschweiler, R.; Ernst, R. R. *Biochemistry* **1997**, *36*, 13043−13053.
(77) Babu, K. R.; Moradian, A.; Douglas, D. J. *J. Am. Soc. Mass Spectrom.* **2000**, *12*, 317−328.
(78) Shi, H.; Pierson, N. a.; Valentine, S. J.; Clemmer, D. E. *J. Phys. Chem. B* **2012**, *116*, 3344−3352.
(79) Eschweiler, J. D.; Martini, R. M.; Ruotolo, B. T. *J. Am. Chem. Soc.* **2017**, *139*, 534−540.
(80) Shi, H.; Clemmer, D. E. *J. Phys. Chem. B* **2014**, *118*, 3498−3506.
(81) Loo, R. R. O.; Loo, J. A. *J. Am. Soc. Mass Spectrom.* **2016**, *27*, 975−990.
(82) Skinner, O. S.; McLafferty, F. W.; Breuker, K. *J. Am. Soc. Mass Spectrom.* **2012**, *23*, 1011−1014.
(83) Servage, K. A.; Silveira, J. A.; Fort, K. L.; Clemmer, D. E.; Russell, D. H. *J. Phys. Chem. Lett.* **2015**, *6*, 4947−4951.
(84) Kristariyanto, Yosua A.; Choi, S.-Y.; Rehman, S.; Arif, A.; Ritorto; Maria, S.; Campbell; David, G.; Morrice; Nicholas, A.; Toth, R.; Kulathu, Y. *Biochem. J.* **2015**, *467*, 345−352.
(85) Kristariyanto, Yosua A.; Abdul Rehman, Syed A.; Campbell, David G.; Morrice, Nicholas A.; Johnson, C.; Toth, R.; Kulathu, Y. *Mol. Cell* **2015**, *58*, 83−94.
(86) Pan, M.; Gao, S.; Zheng, Y.; Tan, X.; Lan, H.; Tan, X.; Sun, D.; Lu, L.; Wang, T.; Zheng, Q.; Huang, Y.; Wang, J.; Liu, L. *J. Am. Chem. Soc.* **2016**, *138*, 7429−7435.
(87) Komander, D.; Reyes-Turcu, F.; Licchesi, J. D. F.; Odenwaelder, P.; Wilkinson, K. D.; Barford, D. *EMBO Rep.* **2009**, *10*, 466−473.

DOI: 10.1021/acs.analchem.7b02932
Anal. Chem. XXXX, XXX, XXX−XXX